ARCHEAN CRATONS: TERMS, CONCEPTS, AND ANALYTICAL APPROACHES

Paul A. Mueller[1] and Carol D. Frost[2]

DOI: 10.2138/gselements.20.3.157

The articles in this *Elements* issue highlight various aspects of the formation and evolution of the Earth's earliest crust. This Toolkit includes a glossary of terms, concepts, and analytical approaches important to the study of Archean cratons to provide context for the methodologies discussed in these articles.

TIMESCALE OF EARLY EARTH

Geologic timescales are rarely presented without compressing the Precambrian portion of Earth history. For this reason, it is easy to overlook the fact that the time between Earth formation and the end of the Archean at 2.5 Ga (billion years ago)—the time period covered by the articles in this issue—represents fully 45% of Earth history (Fig. 1).

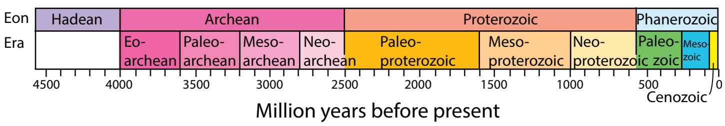

Figure 1 Geologic timescale.

The geologic timescale for the earliest part of Earth history is divided into two eons: the Hadean (4.6 to 4.0 Ga) and the Archean (4.0 to 2.5 Ga) (Fig. 1). The Hadean is defined as the time from Earth formation to the earliest part of the rock record. We use the 4.568 billion-year-old age of the oldest grains condensed from the solar nebula found in meteorites (Ca-Al-rich grains included in chondritic meteorites) to mark the start of Earth accretion (Bouvier and Wadhwa 2010). The beginning of the Archean has been established at 4.031 Ga based on the 10 oldest U-Pb zircon ages from the Acasta gneiss complex in the Slave craton of northern Canada (Bowring and Williams 1999). Consequently, we refer to all ages older than this as Hadean.

The Archean eon is divided into the Eoarchean (4.03–3.6 Ga), the Paleoarchean (3.6–3.2 Ga), the Mesoarchean (3.2–2.8 Ga), and the Neoarchean (2.8–2.5 Ga). Unlike the Phanerozoic, where the timescale is related to the evolution of fossil life forms, these time divisions are arbitrary, as is the end of the Archean eon at 2.5 Ga. The geologic timescale is updated periodically by the International Commission on Stratigraphy (www.iugs.org/ics).

EARTH'S COMPOSITION AND RESERVOIRS

It is not possible to determine the average geochemical composition of the entire Earth directly, so its overall composition—often expressed as the bulk Earth composition—is estimated from the composition of Type-1 carbonaceous chondrite meteorites, a class of meteorites that is thought to have formed during condensation of the solar nebula and formation of the Solar System and has not undergone melting or metamorphism since that time. This composition is also referred to as the chondritic uniform reservoir (CHUR).

1 Department of Geological Sciences
University of Florida
Gainesville, FL 32611, USA
E-mail: pamueller@ufl.edu

2 Department of Geology and Geophysics
University of Wyoming
Laramie, WY 82071, USA
E-mail: frost@uwyo.edu

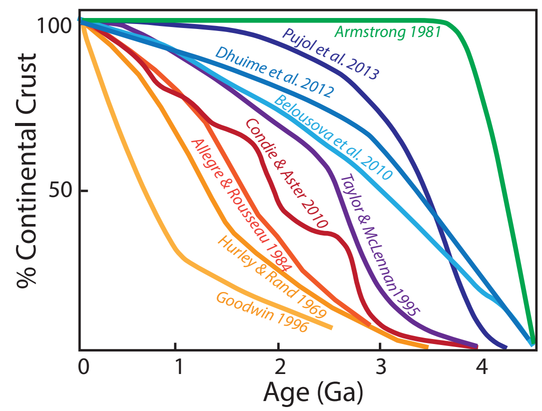

Figure 2 Crustal growth models. Estimates of the time at which the crust first separated from the mantle vary greatly, as does the volume of crust present throughout Earth history, which on this figure is expressed as a percentage of present-day crustal volume. This figure illustrates a variety of models ranging from those that envision abundant crust formation early in Earth history (i.e., green curve) to many other models that suggest that the volume of continental crust has increased over time, albeit at different rates. Modified from Hawkesworth et al. (2019).

Very early in its history, the metallic core separated from the silicate portion of the Earth (Nimmo and Kleine 2015). Thus, it is useful to define the geochemical composition of the bulk silicate Earth as the composition of the entire Earth minus the core. The composition of the bulk silicate Earth is equivalent to that of the primitive mantle.

Today, the Earth is composed of a number of geochemically distinct components, including the core, mantle, and crust. These are commonly referred to as reservoirs. The portion of the mantle that partially melted to produce magmas that contributed to forming the Earth's crust is known as the depleted mantle. The time when the depleted mantle reservoir began to form and the evolution of its composition and volume over Earth history are intricately related to the formation and evolution of the complementary crustal reservoir (Fig. 2). These processes are incompletely resolved in time and space, as discussed by O'Neil et al. (2024 this issue) and Rey et al. (2024 this issue).

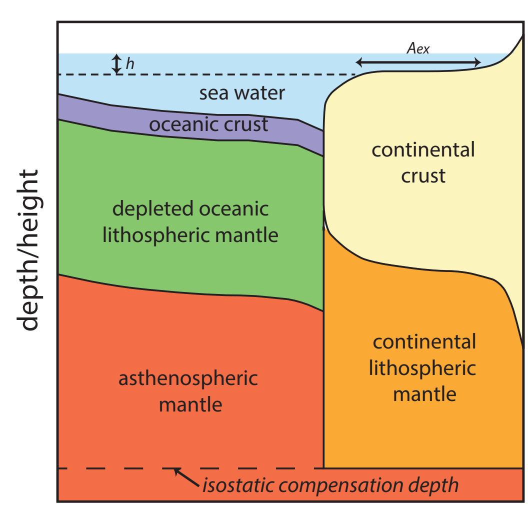

Figure 3 Schematic illustration of continental freeboard (Korenaga et al. 2017). If sea level rises by height h, more of the continental shelf will be submerged, the area of exposed landmasses decreases by area A_{ex}, and continental freeboard decreases.

The Earth's oceans constitute another reservoir that appears to have formed early, likely by 3.7–3.8 billion years ago when pillow basalts are first preserved in the rock record (Nutman et al. 2013). The concept of crustal growth is intimately linked to the concept of continental freeboard, which refers to the mean height of the continental landmasses with respect to sea level at any given time (FIG. 3; Korenaga et al. 2017). This concept is important because freeboard reflects a balance between the volume of the oceans, the shape of ocean basins, and the volume, density, and thickness of the oceanic and continental crust. See Rey et al. (2024 this issue) for a broader discussion of changes in sea level during the Archean.

GEODYNAMICS OF THE EARLY, NON-UNIFORMITARIAN EARTH

Geologic processes are commonly assumed to be *uniformitarian*, that is, we can infer how ancient rocks were formed and modified by looking at modern processes, including plate tectonics, that affect the Earth today. This assumption cannot be applied to the first 1.5 to 2 billion years of Earth history. For example, the formation of Earth's core, silicate magma oceans, and the Moon were early, one-time events. Exponential, secular cooling of the Earth as radioactive heat production decreased produced different temperature regimes at different times in the past (Korenaga 2013). This cooling also likely affected Earth's geodynamics, a general term that refers to the physical stresses that deform Earth's surface and interior. Instead of stiff plates of crust moving horizontally above a convecting mantle in a modern so-called mobile lid process, Hadean and Archean tectonics may have been driven by mantle plumes beneath a weaker, stationary crust, in a so-called stagnant-lid scenario (FIG. 4A). Instead of subduction, the early crust may have been disrupted and even relocated in response to mantle upwellings and downwellings that have been linked to processes such as sagduction and drip tectonics (FIG. 4B; Martin and Arndt 2021).

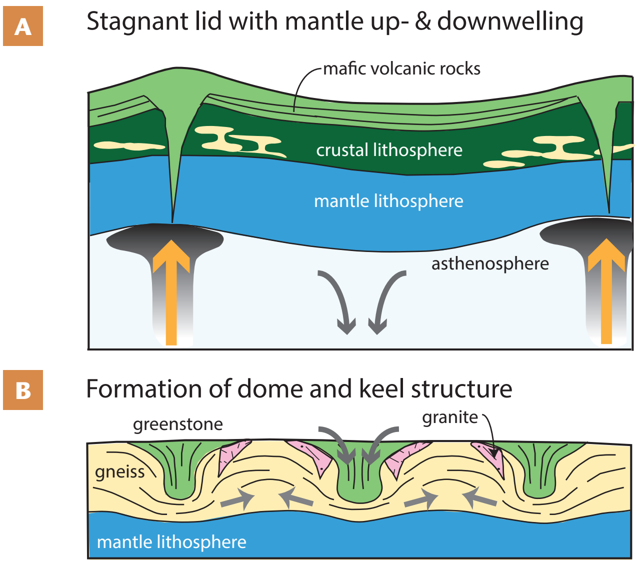

FIGURE 4 Earth currently dissipates >90% of its internal heat via a "multi-plate mobile lid" system (plate tectonics) driven by the sinking of cold dense lithosphere into the convecting mantle. In the Archean-Hadean, higher mantle temperatures and more rapid convective heat loss may have occurred in a "stagnant lid" system, which transitioned to plate tectonics over time. Two possible transitional stages include: (**A**) Hadean mafic crust with nascent TTG differentiates (yellow) formed over broad mantle upwellings (orange arrows) and (**B**) An Archean stage when dense volcanic rocks of greenstone belts sank through warm, weak felsic crust, displacing older felsic crust as diapirs with melt (purple) that intruded the foundering greenstones. This process, often labeled "sagduction," produced the dome and keel pattern shown in FIGURE 2. of Frost and Mueller (2024 this issue).

In addition, studies of the lunar surface indicate by analogy that impacts of large, extraterrestrial bodies (e.g., planetesimals and large meteorites) strongly affected the early Earth, but the rate of these impacts tailed off by the end of the Archean (see recent compilation on FIG. 2 in Tai Udovicic et al. 2023). Large impacts on the early Earth, including the Moon-forming impact, may have generated enough heat to wholly or partially melt large parts of the mantle. The resulting "magma oceans" may have persisted for millions of years and greatly influenced the chemical and physical evolution of the mantle.

The time at which modern plate tectonics initiated is a subject of considerable debate (Korenaga 2013). As Rey et al. (2024 this issue) point out, it is possible that there was a period when both stagnant and mobile tectonic processes were operating in parallel, a situation they refer to as dual-mode geodynamics. The transition from stagnant to mobile lid tectonics need not have been synchronous globally, but likely occurred at different times in different parts of the Earth and affected individual cratons differently (Frost and Mueller 2024 this issue).

AGE DETERMINATIONS OF ARCHEAN AND HADEAN EVENTS

U-Pb in Zircon

The U-Pb system in zircon has evolved to become the most reliable method for obtaining accurate and precise ages of events in the geologic past, particularly the Precambrian. The two radioactive isotopes of uranium (^{235}U and ^{238}U) decay at vastly different rates, providing two independent age determinations and an opportunity to compare ages from one decay system to the other in a unique cross-check. When the ages agree within analytical errors, the ages are considered concordant, implying that the zircon has behaved as a closed system since it formed. The data are often depicted on concordia diagrams, on which curved lines give the ages of concordant data regardless of the ratios used to define concordia. Two different common concordia plots are shown in FIGURE 5. Discordant ages (ages from the two decay systems that do not agree) are also valuable because the lack of agreement often can be related to loss of Pb from the system (e.g., a zircon grain). Straight lines through discordant points (discordia; FIG. 5) on the concordia plots may intersect concordia at two times, and can then identify both the time of original crystallization and the time of the event that caused Pb-loss, such as metamorphism. Because ancient zircons likely experienced more than one Pb-loss event, the lower intercept of the discordia line with concordia may have only limited or no geologic meaning.

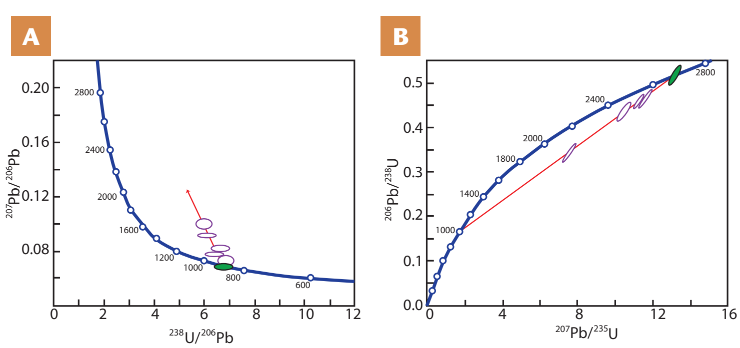

FIGURE 5 Two commonly used types of concordia diagrams. (**A**) Tera-Wasserburg concordia diagram and (**B**) Wetherill concordia diagram. In each, the concordia is shown as the blue curve. Samples plotting on the concordia (green ellipses) give the same age in both the $^{238}U \rightarrow ^{206}Pb$ and $^{235}U \rightarrow ^{207}Pb$ decay systems. Arrays of discordant points (open purple ellipses) may form a chord (discordia) that intersects the concordia at the crystallization age. See FIGURE 4 in Laurent et al. (2024 this issue) for an example of data interpreted on a Tera-Wasserburg diagram.

Common Pb and the Age of the Earth

Common Pb isotopes are those found in "common" rocks and minerals that have not necessarily remained closed systems since they formed. The Pb isotopes produced by decay of ^{235}U (^{207}Pb) and ^{238}U (^{206}Pb) are typically reported as ratios relative to the non-radiogenic isotope ^{204}Pb. Lead produced from decay of ^{232}Th is similarly reported as ^{208}Pb/^{204}Pb from the single decay of ^{232}Th to ^{208}Pb. The Pb isotopic composition of an individual rock or mineral evolves with time to higher ratios of radiogenic Pb (^{206}Pb, ^{207}Pb, ^{208}Pb) to non-radiogenic ^{204}Pb along curved paths called growth curves (FIG. 6). The relatively rapid decay of ^{235}U means that ~80% of all ^{235}U on Earth had decayed by the end the Archean and is the reason why the growth curves shown on FIGURE 6 flatten out at younger ages. Consequently, rocks and minerals with high ^{207}Pb/^{204}Pb relative to ^{206}Pb/^{204}Pb indicate interaction with high-U/Pb reservoir(s) that must have formed in the Hadean or Archean. These are referred to as high-μ or early enriched reservoirs. These reservoirs likely formed by magmatic differentiation within the crust because U is preferentially partitioned into magmas to a greater extent than Pb in crustal and mantle melts.

Common Pb isotopes have played an important role in our evolving understanding of Earth and Solar System history. For example, Pb isotopic data from galenas, oceanic sediments, and meteorites were combined to provide the first viable determination of the age of the Earth (FIG. 6B; Patterson 1956).

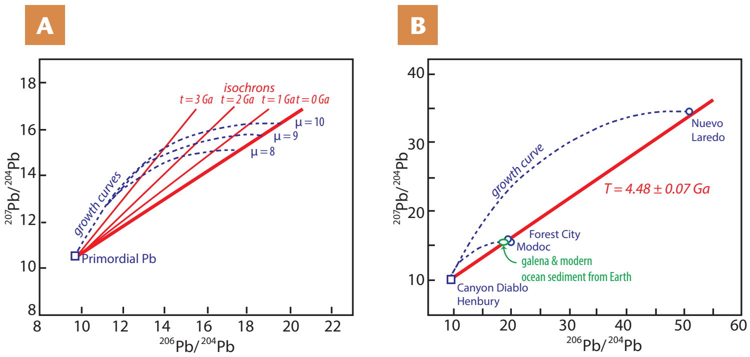

FIGURE 6 (**A**) Evolution of Pb isotopes in Earth reservoirs with different U/Pb ratios (μ = ^{238}U/^{204}Pb) over Earth history from an initial bulk Earth Pb isotopic composition estimated from iron meteorites (Blichert-Toft et al. 2010). At any given time, rocks from reservoirs of the same age, but with different μ-values, will define a straight line (an isochron) with a slope that is a function of age. (**B**) The slope of the red line defined by the Pb isotopic composition of meteorites (blue symbols; blue square = iron meteorites; blue circles = stony meteorites) gives the time of Solar System formation. Because average deep-sea sediment, taken as a proxy for average continental crust, and recently formed galena samples (μ = zero) from ore deposits lie on the same isochron as meteorites, the Earth and meteorites were interpreted to have the same age (Patterson 1956).

ISOTOPIC SYSTEMS USED TO INFER EARTH DIFFERENTIATION PROCESSES

In addition to the U-Pb system, many other radiogenic parent-daughter isotope pairs are used to determine both the timing and nature of events on Earth. Most of these involve parent isotopes with slow decay rates, such as ^{147}Sm-^{143}Nd (half-life ($T_{½}$) of ^{147}Sm = 107.0 billion years), ^{176}Lu-^{176}Hf ($T_{½}$ of ^{76}Lu = 37.2 billion years), and ^{187}Re-^{187}Os ($T_{½}$ of ^{87}Re = 41.6 billion years). As with Pb isotopes, the daughter isotope is reported relative to a stable isotope of the same element. Examples include ^{143}Nd/^{144}Nd (shown on FIG. 7A), ^{176}Hf/^{177}Hf, and ^{187}Os/^{188}Os. The variation in these ratios for Earth materials is very small, so it has become customary to report measured values relative to a standard such as CHUR (the chondritic uniform reservoir, which approximates the bulk silicate Earth composition). This is called the epsilon notation, and is given by the formula:

$$\varepsilon\mathrm{Nd}(t) = \left[\frac{\left(\frac{^{143}\mathrm{Nd}}{^{144}\mathrm{Nd}}\right)_{\mathrm{sample}(t)}}{\left(\frac{^{143}\mathrm{Nd}}{^{144}\mathrm{Nd}}\right)_{\mathrm{CHUR}(t)}} - 1 \right] \times 10{,}000$$

where (t) is the time of interest. Multiplying by 10^4 results in values for εNd(t) commonly between +15 (depleted mantle) and −50, (old felsic crust), where positive values denote samples with higher ^{143}Nd/^{144}Nd than the bulk Earth, and negative values identify samples with lower ^{143}Nd/^{144}Nd than the bulk Earth (FIG. 7B). This is the case because mantle melts have lower Sm/Nd than the residual (depleted) mantle. Analogous expressions give εHf(t). In the ^{187}Re-^{188}Os system, the γOs(t) notation refers to percent deviation from CHUR of ^{187}Os/^{188}Os (multiplying by 100 instead of 10,000).

When evaluating diagrams and/or text that use the epsilon notation, it is important to remember that the relative rate of change of a sample compared to a model reservoir or another sample is related to the half-life of the parent isotope, the time since mineral/rock formation, the parent/daughter ratio, and the assumptions used to calculate the ε of model reservoirs. For example, the depleted mantle formed at 4.6 Ga with an epsilon of zero and has evolved to a range of values centered about +13 εNd. Evolution diagrams may be plotted with measured isotope ratios (FIG. 7A) or derivative ratios such as epsilons (FIG. 7B). Although Hf and Nd isotopic compositions of rocks and minerals can be measured very precisely today, extrapolating these values back over 3–4 billion years involves uncertainties beyond analytical errors.

Model Ages

As shown in FIGURE 7B, a model age is simply an estimate of the time that a sample was extracted from a model reservoir. For example, a given sample's measured ^{143}Nd/^{144}Nd is extrapolated back in time using

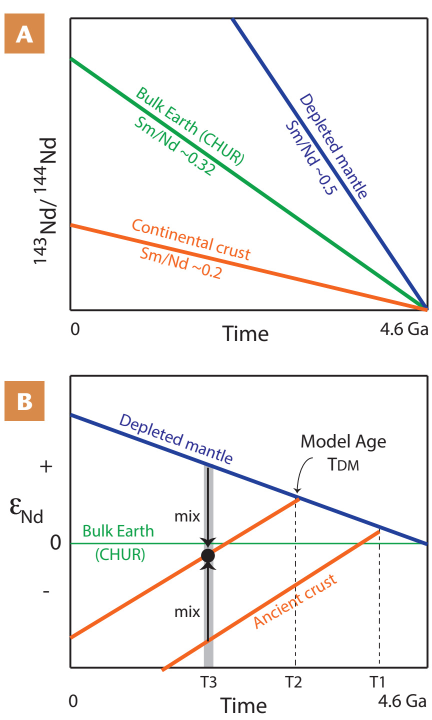

FIGURE 7 The Sm-Nd isotopic system is used to illustrate the change in isotopic composition over time, expressed as the isotopic ratio ^{143}Nd/^{144}Nd (**A**) and epsilon notation (**B**). (**A**) Effect of different Sm/Nd ratios in bulk Earth, crust, and depleted mantle on the accumulation of ^{143}Nd by decay of ^{147}Sm. (**B**) The εNd(t) notation and calculation of model ages. In the example shown, ancient crust formed at time T1 evolves to negative epsilon values, while the depleted mantle evolves to positive epsilon values. At T3, a magma forms by melting and mixing both depleted mantle and crustal sources (black circle). The model age of the mixture is T2. Model ages do not represent the time of a specific event, but instead are a weighted average age of the model sources. FROM MURPHY AND NANCE (2005). See also FIGURE 3 in Laurent et al. (2024 this issue) and FIGURE 3 in O'Neil et al. (2024 this issue).

the sample's measured $^{147}Sm/^{144}Nd$ until its Nd isotopic composition matches that of the evolving reservoir, commonly the depleted mantle. That time is referred to as the depleted mantle model age: T_{DM}. A graphic representation of this concept is shown as point T_{DM} on FIGURE 7B, where the model mantle evolution curve is intersected by the evolution curve of an individual sample at time T2.

Extinct Radionuclides

Some radioactive isotopes produced during stellar processes have such short half-lives that they have completely decayed and are no longer present in our Solar System. These are known as extinct radionuclides. Extinct radionuclides are especially well suited for understanding events that took place on the early Earth while these short-lived radioactive isotopes were still "alive." For example, consider the decay of lithophile (crust-loving) ^{182}Hf ($T_{1/2}$ = 8.9 million years) to siderophile (iron-loving) ^{182}W. In this system, W is fractionated into the core and Hf into the mantle during core formation. The fact that $^{182}W/^{184}W$ is not completely homogenized in the modern mantle after 4.5 Ga of convection and is more heterogeneous in Archean rocks than modern mantle-derived rocks help us understand the timing of core formation and the extent of mantle mixing over time (FIG. 8). Another extinct radionuclide, ^{146}Sm, has also been applied to the chronology of early Archean rocks. Note that instead of the ε notation, the $\mu^{142}Nd(t)$ notation is used with μ referring to parts per million (1×10^{-6}). See O'Neil et al. (2024 this issue) for more discussion.

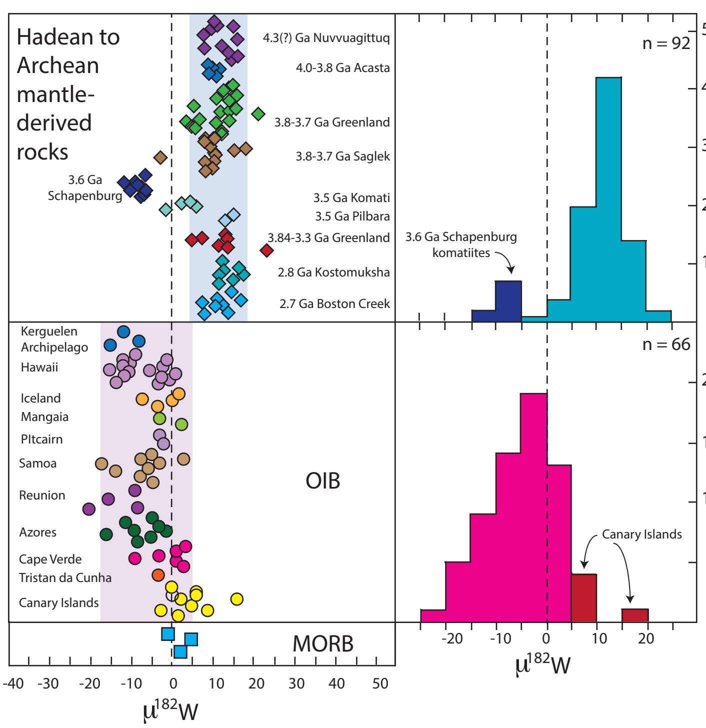

FIGURE 8 Compilation of $^{182}W/^{184}W$ data shown with the $\mu^{182}W$ notation. Data from Hadean and Archean mantle-derived rocks indicate that the Hadean-Archean mantle had $\mu^{182}W$ different from that of modern mantle-derived ocean island basalts (OIB) and mid-ocean ridge basalts (MORB). The difference in $\mu^{182}W$ between Hadean-Archean mantle-derived rocks and modern mantle-derived magmas has been variously attributed to incomplete mantle homogenization in the Archean; core–mantle chemical interaction, possibly related to the crystallization of the inner core; and/or initiation of post-Archean deep slab subduction. FROM RIZO ET AL. (2019).

Oxygen Isotopes

The most abundant element in the silicate Earth is oxygen. The isotopes of oxygen are all stable, yet their abundance varies in Earth materials because the mass difference between isotopes results in different equilibrium and kinetic behavior. A delta notation (δ) is used for oxygen isotope ratios, which most commonly compare the $^{18}O/^{16}O$ of a sample to a standard material, typically "standard mean ocean water" (SMOW), and is expressed as per mil deviations (10^3) from the standard's ratio. Samples with positive $\delta^{18}O$ have higher $^{18}O/^{16}O$ than the standard, and samples with negative $\delta^{18}O$ have lower $^{18}O/^{16}O$ than the standard. In zircon, $\delta^{18}O$ higher than values for the depleted mantle (5.3‰ ± 0.6‰) can indicate incorporation of a sedimentary component and/or interaction of their parent magmas with meteoric water. FIGURE 9 shows a compilation of oxygen isotope data for zircons of different ages depicting a distinct change across the Archean-Proterozoic boundary.

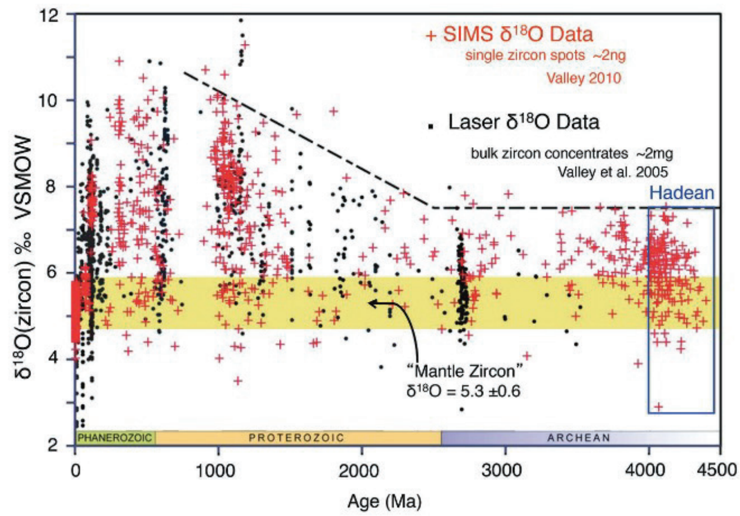

FIGURE 9 Values of $\delta^{18}O$ of zircons plotted as a function of their U-Pb age. Values of $\delta^{18}O$ > 8 are very rare in Archean and Hadean zircons, but rise during the Proterozoic to become much more common in younger samples. SIMS refers to secondary ion mass spectrometry, a method that yields data from an individual micro-domain in the zircon (2 ng as shown). Laser data require much larger samples and are acquired using a laser to heat the sample and then purify the evolved oxygen before analyzing the isotope ratios of the purified gas. REPRODUCED FROM VALLEY ET AL. (2015) WITH PERMISSION FROM THE MINERALOGICAL SOCIETY OF AMERICA.

Presentation of Trace Element Geochemical Data

A common approach to constraining the origin of (meta)igneous and (meta)sedimentary rocks is through the use of trace elements, i.e., elements present below 0.1% by weight. These abundances are often reported in parts per million (ppm) and shown graphically as ratios relative to chondritic meteorites and major Earth reservoirs, such as estimates of the primitive mantle, average crust, average shale, etc. (FIG. 10). The regular behavior of the rare earth elements (REE) is particularly useful because the contraction of ionic size with increasing atomic number leads to predictable behavior in many systems, from igneous to sedimentary. Be aware that the normalizing composition grossly affects the shape of the patterns and that the *y*-axis is always logarithmic. Moreover, the REE are often discussed under the broader term "incompatible elements," which refers to elements that do not readily substitute for the major cations in rock-forming minerals. Depending on a rock's mineralogy, an element may be incompatible in one rock, but not in another.

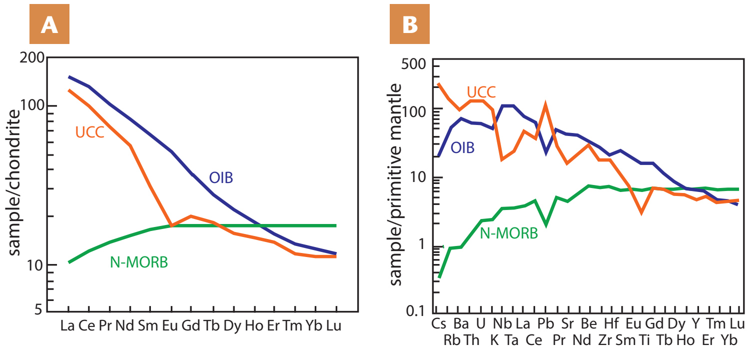

FIGURE 10 (**A**) Rare earth element compositions of typical ocean island basalts (OIB), average upper continental crust (UCC), and normal (depleted) mid-ocean ridge basalt (N-MORB) normalized to the CHUR composition. (**B**) Trace element compositions of typical OIB, UCC, and N-MORB expressed relative to a primitive mantle composition. DATA FROM SUN AND MCDONOUGH (1989), MCDONOUGH AND SUN (1995), LUNDSTROM ET AL. (2003), AND RUDNICK AND GAO (2014). The more irregular pattern for the UCC pattern in (**B**) reflects strong contrasts in the concentrations of many trace elements in accessory minerals such as zircon and monazite that can fractionate from, or accumulate in, more felsic rocks.

GEOPHYSICAL IMAGING OF THE EARTH'S STRUCTURE

Seismic tomography is not only a method to image the Earth's interior, but also a term that refers to a collection of different modeling methodologies centered around an inverse problem. Solutions to inverse problems involve using observations to create a model of the conditions that created the observations. For imaging crustal- or lithospheric-scale structures, tomographic methods are dependent on the number and distribution of seismometers or seismic stations that record the observations. The data recorded on these instruments, such as earthquake waveforms, or even "noise" generated by the oceans, can be used to illuminate the changes in seismic velocities of materials in the subsurface. Body wave tomography, which uses the arrival times of P or S waves, and surface wave tomography, which uses the dispersive nature of Rayleigh or Love waves, have quite different resolutions and sensitivities. The resolution of the models generated is primarily controlled by the wavelength of the seismic waves used in the tomographic inversion, regardless of the specific technique or seismic wave type analyzed. Seismic waves are only sensitive to, or able to detect, heterogeneities that have length scales that are similar to the seismic waves themselves. For example, a 1-second (1-Hz) P-wave with a velocity of 5 km/s has a wavelength of 5 km, which roughly corresponds to the size of the smallest detectable heterogeneity. Surface wave tomography can produce cross sections similar to those shown in FIGURE 3 of Cooper and Miller (2024 this issue). These cross sections are based on much longer wavelength Rayleigh waves, providing lateral resolution on the scale of 10s of kilometers. Because of the way these waves propagate through the Earth, they are most sensitive to lateral variations in the lithosphere and less sensitive to sub-horizontal structures, such as the crust-mantle boundary (Moho). Other types of seismic imaging techniques that use body waves (P and S waves), which travel along more vertical paths, are more sensitive to boundary layers. These methods, typically referred to as receiver functions, are more often used for determining the depth to the Moho or the lithosphere-asthenosphere boundary. Regardless of methodology, these seismic images can then be tested against the temperature and pressure estimates provided by crustal and mantle xenoliths.

REFERENCES

Blichert-Toft J, Zanda B, Ebel DS, Albarède F (2010) The Solar System primordial lead. Earth and Planetary Science Letters 300: 152-163, doi: 10.1016/j.epsl.2010.10.001

Bouvier A, Wadhwa M (2010) The age of the Solar System redefined by the oldest Pb–Pb age of a meteoritic inclusion. Nature Geoscience 3: 637-641, doi: 10.1038/ngeo941

Bowring SA, Williams IS (1999) Priscoan (4.00–4.03 Ga) orthogneisses from northwestern Canada. Contributions to Mineralogy and Petrology 134: 3-16, doi: 10.1007/s004100050465

Cooper CM, Miller MS (2024) Embracing craton complexity at depth. Elements 20: 187-192

Frost CD, Mueller PA (2024) Archean cratons: time capsules of the early Earth. Elements 20: 162-167

Hawkesworth C, Cawood, PA, Dhuime, B (2019) Rates of generation and growth of the continental crust. Geoscience Frontiers 10: 165-173, doi: 10.1016/j.gsf.2018.02.004

Korenaga J (2013) Initiation and evolution of plate tectonics on Earth: theories and observations. Annual Reviews of Earth and Planetary Science 41: 117-151, doi: 10.1146/annurev-earth-050212-124208

Korenaga J, Planavsky NJ, Evans DAD (2017) Global water cycle and the coevolution of Earth's interior and surface environment. Philosophical Transactions of the Royal Society A 375: 20150393, doi: 10.1098/rsta.2015.0393

Laurent O, Guitreau M, Bruand E, Moyen J-F (2024) At the dawn of continents: Archean tonalite-trondhjemite-granodiorite suites. Elements 20: 174-179

Lundstrom CC, Hoernle K, Gill J (2003) U-series disequilibria in volcanic rocks from the Canary Islands: plume versus lithospheric melting. Geochimica et Cosmochimica Acta 67: 4153-4177, doi: 10.1016/S0016-7037(03)00308-9

Martin H, Arndt N (2021) Sagduction. In: Gargaud M and 9 co-editors. Encyclopedia of Astrobiology. Springer, Berlin, doi: 10.1007/978-3-642-27833-4_1400-4

McDonough WF, Sun S-S (1995) The composition of the Earth. Chemical Geology 120: 223-253, doi: 10.1016/0009-2541(94)00140-4

Moore WB, Webb AAG (2013) Heat-pipe earth. Nature 501: 501-505, doi: 10.1038/nature12473

Murphy JB, Nance D (2005) Do supercontinents turn inside-in or inside-out? International Geology Review 47: 591-619, doi: 10.2747/0020-6814.47.6.591

Nimmo F, Kleine T (2015) Early differentiation and core formation: processes and timescales. In: Badro J, Walter MJ (eds) The Early Earth: Accretion and Differentiation. American Geophysical Union, Washington DC, pp 83-102, doi: 10.1002/9781118860359.ch5

Nutman AP, Bennett VC, Friend CRL (2013) The emergence of the Eoarchean proto-arc: evolution of a *c.* 3700 Ma convergent plate boundary at Isua, southern West Greenland. Geological Society, London, Special Publications 389: 113-133, doi: 10.1144/SP389.5

O'Neil J, Rizo H, Reimink J, Garçon M, Carlson RW (2024) Earth's earliest crust. Elements 20: 168-173

Patterson C (1956) Age of meteorites and the earth. Geochimica et Cosmochimica Acta 10: 230-237, doi: 10.1016/0016-7037(56)90036-9

Rey PF, Coltice N, Flament N (2024) Archean geodynamics underneath weak, flat, and flooded continents. Elements 20: 180-186

Rizo H and 9 coauthors (2019) ^{182}W evidence for core-mantle interaction in the source of mantle plumes. Geochemical Perspectives Letters 11: 6-11, doi: 10.7185/geochemlet.1917

Rudnick RL, Gao S (2014) Composition of the continental crust. In: Holland H, Turekian KK (eds) Treatise on Geochemistry, Volume 4 (Second Edition). Elsevier, Oxford, pp 1-51, doi: 10.1016/B978-0-08-095975-7.00301-6

Sun S-S, McDonough WF (1989) Chemical and isotopic systematics of oceanic basalts: implications for mantle composition and processes. In: Saunders AD, Norry MJ (eds) Magmatism in Ocean Basins. Geological Society, London, Special Publication 42: 313-345, doi: 10.1144/GSL.SP.1989.042.01.19

Tai Udovicic CJ and 10 coauthors (2023) Buried ice deposits in lunar polar cold traps were disrupted by ballistic sedimentation. Journal of Geophysical Research: Planets 128: e2022JE007567, doi: 10.1029/2022JE007567

Valley JW and 8 coauthors (2015) Nano- and micro-geochronology in Hadean and Archean zircons by atom-probe tomography and SIMS: new tools for old minerals. American Mineralogist 100: 1355-1377, doi: 10.2138/am-2015-5134 ■